# Enhancing the robustness of underwater dehazing by jointly using polarization and the dark channel prior

Benjamin Le Teurnier, Arnaud Tullio, Matthieu Boffety

# Enhancing robustness of underwater dehazing by jointly using polarization and dark channel prior

BENJAMIN LE TEURNIER ,[1] ARNAUD TULLIO,[2] AND MATTHIEU BOFFETY,[1,*]

[1]*Laboratoire Charles Fabry, Institut d'Optique Graduate School, CNRS, Université Paris-Saclay 11, 91127 Palaiseau, France*
[2] *Innovative Imaging Solutions (i2S), 33600 Pessac, France*
[*]*matthieu.boffety@institutoptique.fr*

**Abstract:** The scattering of light in water generates a veiling effect in underwater images, which significantly reduces visibility and limits the range of imaging systems, particularly in target detection applications. Several dehazing techniques have been developed based on the assumption that the veil and the scene of interest exhibit distinct physical properties, either colorimetric or polarimetric. However, these approaches tend to lose effectiveness when the underlying assumptions are not met. In this study, we propose a method that jointly exploits both the colorimetric and polarimetric characteristics of the veil to enhance image contrast. The proposed approach is evaluated on in-situ images acquired using an underwater imaging system in both passive and active configurations. We demonstrate that our method enables the automatic identification of pixels associated with the veil, facilitating the estimation of its physical properties, and reduces potential ambiguities between the veil and regions of the scene of interest. Experimental results show that our approach achieves performance comparable to conventional techniques while offering improved robustness.

## 1. Introduction

Underwater images are usually perturbed by the turbidity or scattering properties of the medium. The scattering of the light in a turbid medium creates a veil that reduces the contrast and the visibility range. This makes it difficult to discern the elements in the scene within the acquired image [1]. To address this issue, various processing methods have been proposed to dehaze the images. Some of these methods use contrast enhancing techniques such as contrast limited adaptive histogram equalization (CLAHE) [2] to improve the visibility in the images [3]. The use of colorimetric information within the image has also been successfully used to develop dehazing techniques, such as the dark channel prior (DCP) method [4, 5].

The use of polarization has also been investigated. Experimentation to reduce back-scattering by using circularly polarized light was conducted decades ago by Gilbert *et al* [6]. However, due to the difficulty to use circular polarization state analyses on field experiments, linear polarization state analyses have been mostly used since. A dehazing method using two orthogonal linear polarization states analysis was developed by Schechner *et al* [7] with underwater experiments [8]. Many enhancements of this method have been proposed since [9–13], especially to adapt it to active polarized illumination [14–19]. Several studies [20, 21] also adapt the dehazing method developed by Schechner *et al* to a new kind of polarimetric sensor. This new integrated Division of Focal Plane (DoFP) sensor enables four polarimetric analyses in a single acquisition [22]. Moreover, it has been shown that the DCP dehazing method can be applied on the results of a polarimetric camera using a polarized illumination and a polarized analysis with orthogonal states [23]. The DCP dehazing method has also been applied on the polarimetric measurements before the estimation of the polarization state of the remaining light in order to help the detection of objects obscured by the hazy veil [24].

Both standard DCP and polarimetric methods relies on the assumption that the scattering veil and the scene of interest exhibit distinct physical properties, colorimetric or polarimetric respectively. When this assumption is violated – when regions of the scene exhibit properties similar to the veil – ambiguities arise and may lead to suboptimal dehazing results. In this paper, we propose a method that simultaneously integrates colorimetric and polarimetric information acquired from a DoFP sensor, rather than processing them separately or sequentially. This approach fully leverages the capabilities of the DoFP sensor. Furthermore, it has been experimentally validated on a DoFP polarimetric imaging system developed for underwater target detection, both in passive or active configurations. We demonstrate that our method effectively mitigates the aforementioned ambiguities. We also quantify its performance—relative to conventional techniques—using a straightforward contrast metric and a statistical distance measure that accounts for noise and show that it achieves performance comparable to conventional techniques.

The article is organized as follows. In the second section, we briefly describe the basis of the light propagation model used to dehaze the images. In the third and fourth sections, we briefly recall the basis of Schechner's polarimetric method and the DCP method on which our work relies. In the following section we detail our dehazing method, we demonstrate how to simultaneously use the benefits of the two previous methods to enhance the robustness of dehazing. In Section 6, we present the experimental set-up we used to acquire the underwater images as well as the protocol we followed to compare our approach to conventional techniques. Finally, in the last section, we present the dehazing results obtained with the different methods on passive and active imaging scenarios.

## 2. Light propagation model

For our study, we rely on a physical model of light propagation in water that has been widely used to address the dehazing problem [4, 5, 7–21, 23]. It was first introduced for aerial imaging but was successfully applied to underwater images as it can similarly describe the scattering of light in the air and underwater.

Figure 1 describes the origin of the veil due to the scattering of the illumination light. The light incident on the camera $I$ is a superposition of the light from the veil due to the medium with intensity $A$ and the light from the scene transmitted through the scattering medium with intensity $D$. Thus, the light intensity measured by a camera pixel of coordinate $x$ can be written as

$$I(x) = A(x) + D(x). \tag{1}$$

The intensity of the light scattered by the veil is related to the transmission $t$ of the scattering medium. This transmission decays with the distance to the scene. On one hand, one can express the relation between $A(x)$ and $t(x)$ through

$$A(x) = A_\infty[1 - t(x)], \tag{2}$$

where $A_\infty$ is the intensity only coming from the veil defined as the intensity of a point where the scene is at an infinite distance. It is supposed constant on the whole image. One the other hand, the intensity coming from the scene transmitted through the scattering medium is expressed by

$$D(x) = L(x)t(x). \tag{3}$$

The intensity $L(x)$ of the light coming from the scene can therefore be easily deduced as

$$L(x) = \frac{I(x) - A(x)}{t(x)}. \tag{4}$$

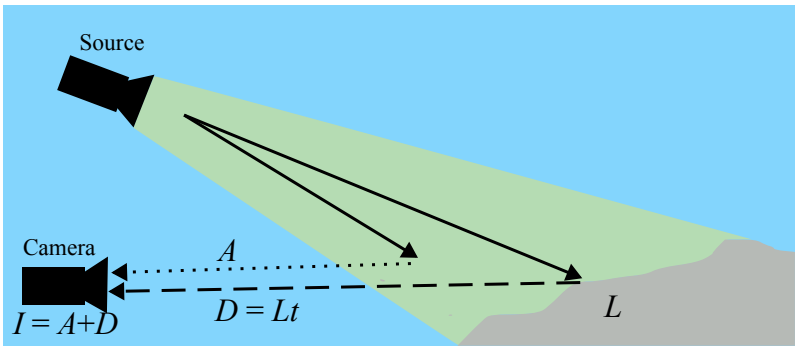


Fig. 1. Diagram of the scattering of the light. $L$ is the light reflected by the scene toward the camera, $D$ is the part of this light transmitted through the scattering medium of transmission $t$ and $A$ is the light from the illumination scattered by the medium toward the camera. The illumination light may originate either from an active source or from the sun in the case of passive imaging. Furthermore, no assumption is made regarding the polarization state of the illumination.

The parameters $I(x)$, $A(x)$ and $t(x)$ are thus to be estimated in order to retrieve the dehazed image $L$.

One drawback we faced while using Eq. (4) is that the dynamic of the dehazed image $L$ can become greater than the dynamic of the original image $I$. This might lead to a decrease of the contrast on important parts of the image. To highlight this behavior, we rewrite Eq. (4) as

$$L(x) = g(x)I(x), \tag{5}$$

where $g(x)$ is a gain defined by

$$g(x) = \frac{A_\infty}{I(x)} \frac{I(x) - A(x)}{A_\infty - A(x)}. \tag{6}$$

The gain $g(x)$ exceeds 1 when $A_\infty < I(x)$, which occurs when an object located close to the camera—hence only weakly affected by the scattering veil—is brighter than the most veiled regions of the image. In such cases, applying a gain greater than 1 increases the brightness of these already bright pixels. Consequently, for a given dynamic range, darker regions may appear even darker by contrast, resulting in a loss of visibility in hazy areas and a global reduction in image contrast. To mitigate this effect, we constrained the gain $g(x)$ to a maximum value of 1 through thresholding.

## 3. Dehazing using the polarization of light

Mainly known through the work of Schechner *et al* [7–9], the use of polarization to dehaze underwater images relies on the assumption that the light scattered by the medium creating the veil and the light scattered by the scene of interest are polarized differently: the former is polarized whereas the latter is unpolarized [7–15, 17–21, 23]. In this context, the intensity of the veil can be estimated using the acquisitions of two orthogonal polarized states, denoted $I^{\parallel}$ and $I^{\perp}$,

$$A(x) = \frac{I^{\parallel}(x) - I^{\perp}(x)}{P_{\mathrm{A}}}, \tag{7}$$

where $P_{\mathrm{A}}$ is the partial (usually linear) degree of polarization of the veil which is supposed to be constant over the image. Both $P_{\mathrm{A}}$ and $A_\infty$ can be estimated in an area of the image where there is

only light coming from the veil, meaning that $I^{\parallel} = A^{\parallel}$ and $I^{\perp} = A^{\perp}$, with

$$P_{\mathrm{A}} = \frac{A^{\parallel}(x) - A^{\perp}(x)}{A^{\parallel}(x) + A^{\perp}(x)}, \tag{8}$$

$$A_{\infty} = A^{\parallel}(x) + A^{\perp}(x). \tag{9}$$

Using Eqs. (7) and (9), one can estimate $t(x)$ through Eq. (2) and the dehazed image through Eq. (4).

The use of polarimetric Division of Focal Plane (DoFP) sensors [22] gives access to four different analysis states denoted $I_0$, $I_{45}$, $I_{90}$ and $I_{135}$ referring to linearly polarized analysis states oriented respectfully at 0°, 45°, 90° and 135°. One can thus use the associations of ($I_0$, $I_{90}$) or ($I_{45}$, $I_{135}$) as orthogonal analysis state measurements ($I^{\parallel}$, $I^{\perp}$). If methods have been proposed to adapt the polarimetric dehazing method to this kind of sensors, to our knowledge none used the capacity of the sensor to its full extent. Indeed, these sensors allow one to estimate the full linear Stokes vector of the light $\mathbf{S} = [S_0, S_1, S_2]^T = [S_0, S_0P\cos(\theta), S_0P\sin(\theta)]^T$ where $S_0$ denotes the total intensity, $P$ the degree of linear polarization (DoLP) and $\theta$ the angle of polarization (AoP). The DoLP is computed with $P = \sqrt{S_1^2 + S_2^2}/S_0$ and the AoP with $\theta = \arctan(S_2/S_1)$.

The linear Stokes vector of the incident light is equal to the sum of the Stokes vector of the back scattered light (forming the veil) and the Stokes vector of the light from the scene which leads to

$$I(x)P(x)\cos(\theta(x)) = A(x)P_{\mathrm{A}}(x)\cos(\theta_{\mathrm{A}}(x)) + D(x)P_{\mathrm{D}}(x)\cos(\theta_{\mathrm{D}}(x)), \tag{10}$$

and

$$I(x)P(x)\sin(\theta(x)) = A(x)P_{\mathrm{A}}(x)\sin(\theta_{\mathrm{A}}(x)) + D(x)P_{\mathrm{D}}(x)\sin(\theta_{\mathrm{D}}(x)), \tag{11}$$

where $P(x)$ and $\theta(x)$ are the DoLP and AoP of the measured intensity, $P_{\mathrm{A}}(x)$ and $\theta_{\mathrm{A}}(x)$ are the DoLP and AoP of the veil and $P_{\mathrm{D}}(x)$ and $\theta_{\mathrm{D}}(x)$ are the DoLP and AoP of the light coming from the scene. Under the previous assumption that the light coming from the scene is unpolarized, one as $P_{\mathrm{D}}(x) = 0$ and $\theta(x) = \theta_{\mathrm{A}}(x)$. Then, by considering that the veil is uniformly polarized, $P_{\mathrm{A}} \neq 0$ leads to

$$A(x) = \frac{I(x)P(x)}{P_{\mathrm{A}}}, \tag{12}$$

where $I(x)$ and $P(x)$ are estimated on each pixel of the image from the measurements. The DoLP of the veil $P_{\mathrm{A}}$ is estimated by choosing the estimated DoLP on a zone of the image where the veil is the only source of incident light. The intensity of the veil $A_{\infty}$ is also estimated on this region from the estimated total intensity $S_0$. As previously, we can use these estimations to dehaze the image according to Eq. (4).

One limitation of this model is therefore its assumption that the light reflected by the scene is unpolarized. This assumption may not hold in active configurations involving polarized illumination and scenes with manufactured objects. In such cases, the dehazing method may incorrectly treat these objects as part of the scattering veil, as illustrated in one of our case studies (Figure 6 of Section 7.2). For such cases, it might be necessary to identify an alternative strategy. In particular, we show in Section 7.2 that the approach we propose in this study might help mitigate such ambiguities.

Another challenge of this method is that it does not enable to automatically find the area in the image where to estimated $A_{\infty}$ and $P_{\mathrm{A}}$ without the supervision of an operator. One way to alleviate this issue is to rely on the Dark Channel prior method.

## 4. Dark Chanel prior (DCP)

The DCP dehazing method [4, 25] uses the colorimetric properties of the scene to estimate the transmission of the scattering medium. This prior states that, in a scene without the veil due

to the scattering of light, at least one of the colorimetric channels of one pixel in a given area receives a low – if not null – intensity. On the contrary, in the presence of the veil, the lowest intensity among the colorimetric channels in the same area will be of a higher value. The dark channel prior therefore allows at the same time to identify the pixels corresponding to the veil in the image and to estimate the global parameters $A_\infty$ and $t$ of the veil, allowing to dehaze the image through Eqs. (2) to (4).

To identify pixels of the veil, we first define the dark channel image as

$$I^{\text{dark}}(x) = \min_{c\in\{r,g,b\}} \left\{ \min_{y\in\Omega(x)} [I^c(y)] \right\}, \tag{13}$$

where the superscript $c$ denotes the considered colorimetric channel and $\Omega(x)$ is a neighborhood centered on the coordinate $x$. In the case of an image $I$ undisturbed by the veil, the resulting dark channel image $I^{\text{dark}}$ shall be close to zero everywhere. On the contrary, a hazy image $I$ will lead to a dark channel image $I^{\text{dark}}$ with higher values. One can use this prior to select the pixels corresponding to the veil only. Those pixels are found where $I^{\text{dark}}$ is the highest. This enables the estimation of the parameter $A^c_\infty$ of the veil for each colorimetric channels. Therefore, if one chooses a set of pixels $\boldsymbol{\theta}$ with the highest values of $I^{\text{dark}}$, those pixels will correspond to pixels of the veil and enable to estimate $A^c_\infty$ through

$$A^c_\infty = \langle I^c \rangle_{\boldsymbol{\theta}}, \tag{14}$$

where $\langle\cdot\rangle_{\boldsymbol{\theta}}$ denotes the average over the set of pixels $\boldsymbol{\theta}$. In our study, we chose the 1000 brightest pixels of $I^{\text{dark}}$.

To estimate the transmission $t$ of the veil [4], we reformulate the scattering model described in Eq. (4) as

$$I(x) = L(x)t(x) + A_\infty(1 - t(x)). \tag{15}$$

For each colorimetric channel independently, we take the minimum over the neighborhood $\Omega(x)$ in Eq. (15):

$$\min_{y\in\Omega(x)} \{I^c(y)\} = \min_{y\in\Omega(x)} \{L^c(y)\}\, t(x) + (1 - t(x))A^c_\infty. \tag{16}$$

Assuming $t$ is constant over the neighborhood $\Omega(x)$, we then take the minimum among the 3 colorimetric channels after dividing by the intensity of the veil at the infinite $A^c_\infty$:

$$\min_{c\in\{r,g,b\}} \left\{ \min_{y\in\Omega(x)} \left\{ \frac{I^c(y)}{A^c_\infty} \right\} \right\} = \min_{c\in\{r,g,b\}} \left\{ \min_{y\in\Omega(x)} \left\{ \frac{L^c(y)}{A^c_\infty} \right\} \right\} t(x) + (1 - t(x)). \tag{17}$$

The dark channel prior applied on the dehazed image $L$ leads to

$$L^{\text{dark}}(x) = \min_{c\in\{r,g,b\}} \left\{ \min_{y\in\Omega(x)} [L^c(y)] \right\} = 0, \tag{18}$$

as this image is not hazy and its dark channel shall tends to zero. The non null terms of the Eq. (17) lead to

$$t(x) = 1 - \min_{c\in\{r,g,b\}} \left\{ \min_{y\in\Omega(x)} \left[ \frac{I^c(y)}{A^c_\infty} \right] \right\}. \tag{19}$$

Introducing $\omega$ (with $0 < \omega < 1$), a regularization parameter set to avoid dividing by zero in Eq. (4), we obtain

$$t(x) = 1 - \omega \min_{c\in\{r,g,b\}} \left\{ \min_{y\in\Omega(x)} \left[ \frac{I^c(y)}{A^c_\infty} \right] \right\}. \tag{20}$$

This estimated transmission is then refined using guided image filtering algorithm [25, 26].

## 5. Polarimetric DCP

One drawback of the DCP method is the confusion it can make between the veil and a wide white area of the scene. Any wide white area will be considered part of the veil, even if it is a part of the scene, as it will correspond to the brightest pixels of the dark channel image $I^{\text{dark}}$. We observed this behavior on underwater sand areas. It is illustrated on the image on the top left of Figure 2. On this Figure, we display an intensity image of an underwater scene with a wide bright sand area in the foreground. The pixels selected by the DCP method to estimate the parameters of the veil are marked in red. As we can see, these pixels are part of the sand area instead of being part of the veil which is at the background.

One way to bypass this issue is to realize that most of these white areas in underwater scenes have a great depolarization effect leading to a low estimated DoLP. This is highlighted on the bottom left of Figure 2 which shows the DoLP over the full image in the red channel. As we can see, the veil is polarized with a DoLP between 0.15 and 0.2 whereas the sand in the foreground has a DoLP lower than 0.05. This is also true for the other color channels not shown here. We thus propose to associate the information on the DoLP to the information on the colorimetry used by the DCP method. To do so, we use the dark channel prior on the product $I \times P$ instead of the intensity $I$. This product represents the intensity of the fully polarized part of the light. The red channel of $I \times P$ is displayed on the bottom right of Figure 2. We thus introduce $I \times P$ instead of $I$ in Eq. (13) leading to

$$I_P^{\text{dark}}(x) = \min_{c\in\{r,g,b\}} \left\{ \min_{y\in\Omega(x)} \left[ I^c(y) P^c(y) \right] \right\}, \tag{21}$$

where $I^c$ and $P^c$ are the colorimetric channels of the intensity and DoLP images $I$ and $P$, respectively. We display on the top right image of Figure 2 the pixel selection obtained with this method. The selected pixels are showned in red on the intensity image. As one can see, all the pixels belong to the area of the image containing only the veil, illustrating the ability of our method to alleviate the drawback of the DCP method highlighted above and to obtain a more reliable selection of pixels of the veil in order to estimate its parameters.

We then propose to also include the polarization information into the dehazing part of the DCP method. We begin by reformulating the fully polarized intensity expression given in Eq. (10) using (2):

$$\frac{I^c(x)P^c(x)\cos(\theta^c(x))}{A_\infty^c P_{\text{A}}^c \cos(\theta_{\text{A}}^c(x))} = \frac{D^c(x)P_{\text{D}}^c(x)\cos(\theta_{\text{D}}^c(x))}{A_\infty^c P_{\text{A}}^c \cos(\theta_{\text{A}}^c(x))} + (1 - t(x)), \tag{22}$$

where the superscript $c \in (r, g, b)$ denotes the colorimetric channel, $I^c$ is the measured intensity, $P^c$ and $\theta^c$ are the DoLP and AoP of the measured intensity, $P_{\text{A}}^c$ and $\theta_{\text{A}}^c$ are the DoLP and AoP of the scattering veil which are supposed constant over the scene, $D^c$ the intensity dehazed but not corrected from the medium transmission, $P_{\text{D}}^c$ and $\theta_{\text{D}}^c$ are the DoLP and AoP of the light coming from the scene, $t$ the transmission of the scattering medium and $A_\infty^c$ the intensity of the veil. For each colorimetric channel independently, we take the minimum over a neighborhood $\Omega(x)$ centered on the pixel of coordinate $x$ in Eq. (22). Assuming $t$ is constant over the neighborhood, we obtain

$$\min_{y\in\Omega(x)} \left\{ \frac{I^c(x)P^c(x)\cos(\theta^c(x))}{A_\infty^c P_A^c \cos(\theta_{\text{A}}^c(x))} \right\} = \min_{y\in\Omega(x)} \left\{ \frac{D^c(x)P_D^c(x)\cos(\theta_{\text{D}}^c(x))}{A_\infty^c P_A^c \cos(\theta_{\text{A}}^c(x))} \right\} + (1 - t(x)). \tag{23}$$

Then, we take the minimum among the 3 colorimetric channels:

$$\min_{c\in\{r,g,b\}} \left\{ \min_{y\in\Omega(x)} \left\{ \frac{I^c(x)P^c(x)\cos(\theta^c(x))}{A_\infty^c P_A^c \cos(\theta_{\text{A}}^c(x))} \right\} \right\} = \min_{c\in\{r,g,b\}} \left\{ \min_{y\in\Omega(x)} \left\{ \frac{D^c(x)P_D^c(x)\cos(\theta_{\text{D}}^c(x))}{A_\infty^c P_A^c \cos(\theta_{\text{A}}^c(x))} \right\} \right\} + (1 - t(x)). \tag{24}$$

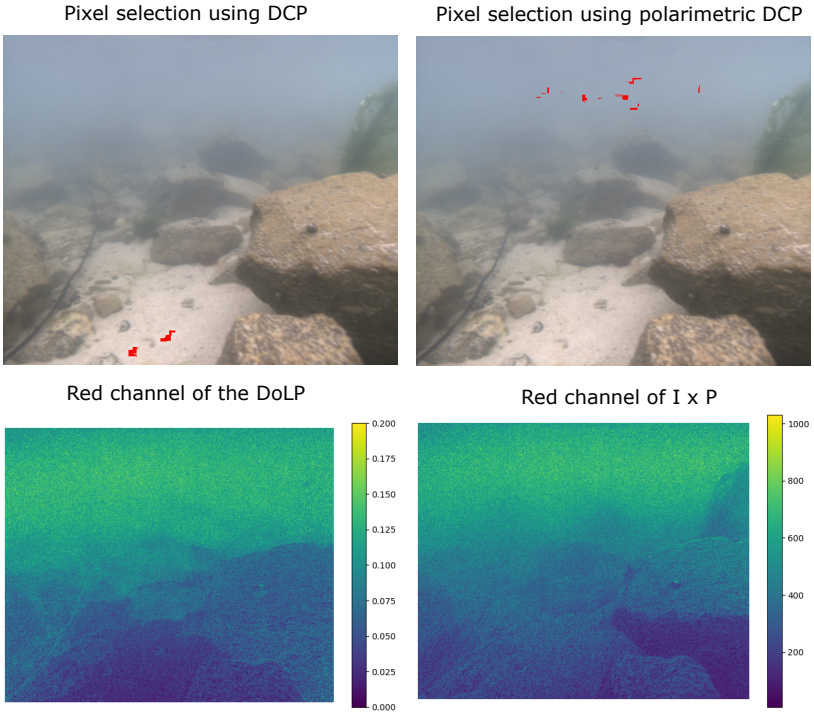


Fig. 2. Upper row: Intensity images of a scene composed of rocks and sand, as well as a veiled area in the background. In red, the pixels selected to estimate the veil parameters using respectively the DCP method (left) and polarimetric DCP method (right). Lower row: Image of the degree of linear polarization for the red channel (left) and image of the product $I \times P$ in the red channel given in number of photo-electrons (right).

On the one hand, the dark channel prior applied to the dehazed image $D$ gives us

$$D^{\text{dark}}(x) = \min_{c\in\{r,g,b\}} \left\{ \min_{y\in\Omega(i,j)} [D^c(y)] \right\} = 0, \tag{25}$$

as this image is not hazy and its dark channel shall tends to zero. On the other hand, the light coming from the scene is supposed unpolarized leading to $P_D^c(x) = 0$ and $\theta^c(x) = \theta_{\text{A}}^c(x)$. For both these reasons, we have

$$\min_{c\in\{r,g,b\}} \left\{ \min_{y\in\Omega(x)} \left\{ \frac{D^c(x) P_D^c(x) \cos(\theta_{\text{D}}^c(x))}{A_\infty^c P_A^c \cos(\theta_{\text{A}}^c(x))} \right\} \right\} = 0. \tag{26}$$

The non null terms of Eq. (24) lead to

$$t(x) = 1 - \min_{c\in\{r,g,b\}} \left\{ \min_{y\in\Omega(x)} \left\{ \frac{I^c(x) P^c(x)}{A_\infty^c P_A^c} \right\} \right\}. \tag{27}$$

Introducing once again the regularization parameter $\omega$ (with $0 < \omega < 1$) to avoid the case where $t(x) = 0$ which leads to a division by zero in Eq. (4), we obtain

$$t(x) = 1 - \omega \min_{c\in\{r,g,b\}} \left\{ \min_{y\in\Omega(x)} \left[ \frac{I^c(y) P^c(y)}{A_\infty^c P_A} \right] \right\}. \tag{28}$$

Combining the dark channel prior and the hypothesis of low DoLP of the light coming from the scene makes the dehazing method more reliable. Particularly, parts of the scene with great fluctuations may leads to errors in the DoLP estimation while using a DoFP camera [27, 28]. In these areas the DoLP is mostly overestimated [28] which makes the estimation to be in contradiction with the hypothesis that the DoLP of the scene is low. In this particular case, the dark channel prior compensates this estimation error of the DoLP. On the other hand, the dark channel prior cannot be applied on white areas of the scene like sand areas. Due to the high depolarization of such areas, the low polarization hypothesis of the scene compensates for this drawback.

## 6. Application on experimental data: imaging setup and comparison criteria

We applied our method to experimental images acquired *in situ* using an underwater polarimetric imaging system operating in passive or active configurations. The objective is to evaluate its performance in comparison with that of conventional dehazing techniques. In this section, we present the experimental setup used as well as the comparison protocol that was implemented.

### *6.1. Experimental imaging setup*

The images used to test our dehazing method were acquired using the Orphiecam underwater polarimetric RGB camera from the company i2S [29]. This camera is equipped with the Sony IMX264MZR CMOS DoFP sensor sensitive to the linear polarization state of the incident light. It enables snapshot measurements of 4 different linear polarization states. Those 4 polarimetric analyses are available for each of the RGB-color channels. Image resolution is 2448 by 2048 pixels.

Images have been acquired using passive and active configurations. The passive configuration consists of the camera alone, the scene being illuminated with natural light in shallow waters. For active imaging, two illumination modules were located on the sides of the camera as we can see on the Figure 3. This Figure shows the polarimetric camera and the two illumination modules placed under a submarine drone.

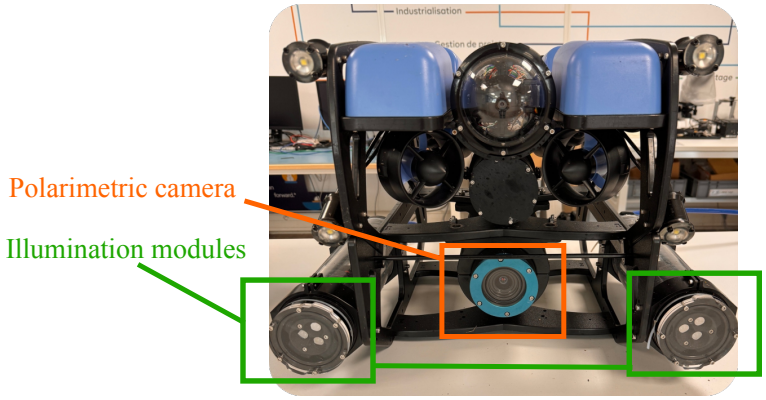


Fig. 3. The imaging system mounted under a submarine drone. The polarimetric camera is placed in the center with the two illumination modules on its sides. The modules can illuminate the scene using linear polarized light at 0°, 45° or 90°. In passive configuration, only the camera is used.

The light provided by the illumination modules was linearly polarized. Three orientations of the polarization states were available: 0°, 45° or 90°. However, in this configuration, the scattering of light by the water enhances the linear polarization with orientation 90° [30]. We

thus decided to use this orientation for the polarized illumination light in order to maximize the degree of polarization of the scattered light.

### 6.2. The methods being compared

For this study, we compared the dehazing performance of the following methods: The polarimetric method described in Section 3, the DCP method described in Section 4, our polarimetric DCP method described in the previous section, the CLAHE (Contrast Limited Adaptive Histogram Equalization) method and simple histogram equalization.

The parameters $A_\infty$ and $P_A$ of the veil used for the DCP method and the polarimetric method were estimated by using the pixel selection obtained with the polarimetric DCP method presented in the previous section. We thus used the same parameters for these three dehazing methods.

The CLAHE method and histogram equalization were applied on the Y channel of the YUV decomposition of the intensity image. We made this choice in order to preserve the color balance of the image.

For each result, we limited the dynamic of the image by applying a threshold to the 1% of the darker pixels and 1% of the brighter pixels respectively to their highest and smallest values. This is also applied to the non dehazed image in the following results for visualization purposes.

### 6.3. Comparison criteria

To compare the performance of the different methods, we proceeded in two stages. First, we conducted a qualitative analysis of the unveiling results, discussing the visual behavior of the various algorithms. In a second stage, we carried out a quantitative comparison based on contrast criteria between two regions of the images. This approach is motivated by the target detection applications (such as demining and offshore inspection) for which the imaging system developed during this study is intended. The comparison was performed using two criteria that can be linked to the Bhattacharyya distance, which is recognized as a reliable contrast metric in the case of noisy optical images for target detection [31].

The first criterion is computed with [32]

$$C_g = \frac{|m_a - m_b|}{\Delta}, \tag{29}$$

where $m_a$ and $m_b$ are respectively the mean value in the two chosen areas $a$ and $b$, and $\Delta$ is the full dynamic range of the image (equal to 1 if the image was normalized into the interval [0, 1]). This easy to use and to interpret criterion can be seen as a global contrast criterion, assuming the same level of noise on all the regions of the image. One drawback is that it does not take into account the noise level in different parts of the image.

In order to have a criterion that takes into account the level of noise, we also computed the Fisher distance [31]:

$$D_F = \frac{(m_a - m_b)^2}{\sigma_a^2 + \sigma_b^2}, \tag{30}$$

where $\sigma_a$ and $\sigma_b$ are the standard deviation of areas $a$ and $b$.

## 7. Application on experimental data: results

We applied our method to two sets of images acquired in either passive or active configurations. In passive configuration, we acquired a set of 135 images by day in shallow waters. For the active configuration, a dataset of 30 images was taken by night. Both sets were acquired off the coast of Brittany. The results presented in this section are representative of the outcomes obtained with both image sets [**?**].

For the quantitative comparison based on the contrast metrics defined in Section 6.3, the results shown in this article were obtained using the red channel of the original images. Analyses conducted on the green and blue channels yielded comparable results, and are not included here for the sake of clarity and space.

### 7.1. Study in passive configuration

Figure 4 shows dehazing results on an image acquired in passive configuration. Each dehazing method results in a significant improvement in visibility, particularly in regions of the image where the presence of the scattering veil is most pronounced—typically corresponding to the most distant parts of the scene. However, these methods impact the overall appearance of the image in different ways. Both CLAHE and histogram equalization produce images with less saturated colors, as they tend to preserve the uniform, low-saturation color balance characteristic of the veil. But, histogram equalization can produce oversaturated values in the foreground, which degrades the visual quality in areas that originally required no restoration. In contrast, the DCP method introduces a noticeable increase in the red channel, altering the color balance. The polarimetric and polarimetric DCP approaches maintain a better color consistency throughout the image, closely matching the characteristics of the foreground.

Figure 5 presents the contrast measurements obtained on the same scene. The image at the top left shows the full scene with a yellow rectangle indicating the zoomed-in region displayed in the other panels of the figure. The red and blue little squares mark the two regions used to compute the contrasts. The remaining panels in the figure present the results obtained with the different dehazing methods. For each method, the histograms corresponding to the pixel intensities within the red and blue regions are shown, along with their mean values and standard deviations, reported in the legend. The subtitles indicate the values of the global contrast $C_g$ and the Fisher distance $D_F$ computed according to Eqs. (29) and (30). The zoomed-in region displayed in each panel and used for the metrics calculation shows the red channel of the corresponding dehazed image.

We computed the metrics between a dark area and a light area on two rocks at the background of the scene where the effect of the veil is most pronounced. On the original image one cannot distinguish these two rocks. The global contrast between the two areas is 0.1 and the Fisher distance is 70.

In the same areas, the images dehazed with the DCP and polarimetric DCP methods exhibit higher global contrast values—0.37 and 0.38, respectively. The polarimetric method yields a slightly lower contrast of 0.29, while the CLAHE method results in a global contrast of 0.21. These values accurately reflect the observed improvements in visibility in the images (cf. Figure 4), where visibility is substantially enhanced by the DCP, polarimetric DCP, and polarimetric methods. In comparison, the CLAHE method produces a more limited enhancement in this area.

However, it is important to note that the DCP, polarimetric DCP, and polarimetric methods also lead to a significant increase in the standard deviation within the selected regions, an effect that is less pronounced with the CLAHE method. As a result, the Fisher distance is higher for CLAHE and is equal to 106, whereas it is reduced to 43, 45, and 31 for the DCP, polarimetric DCP, and polarimetric methods, respectively. This discrepancy between global contrast and Fisher distance measurements indicates that DCP, polarimetric DCP and polarimetric dehazing methods yield greater gains in visibility, but at the expense of increased noise levels.

### 7.2. Study in active configuration

Figure 6 presents results on images acquired by night using the active imaging system presented in Section 6.1. The scenefeature an underwater mine on the seafloor at approximately 1.5 m from the imaging system when the image was acquired. The lower part of the mine is made

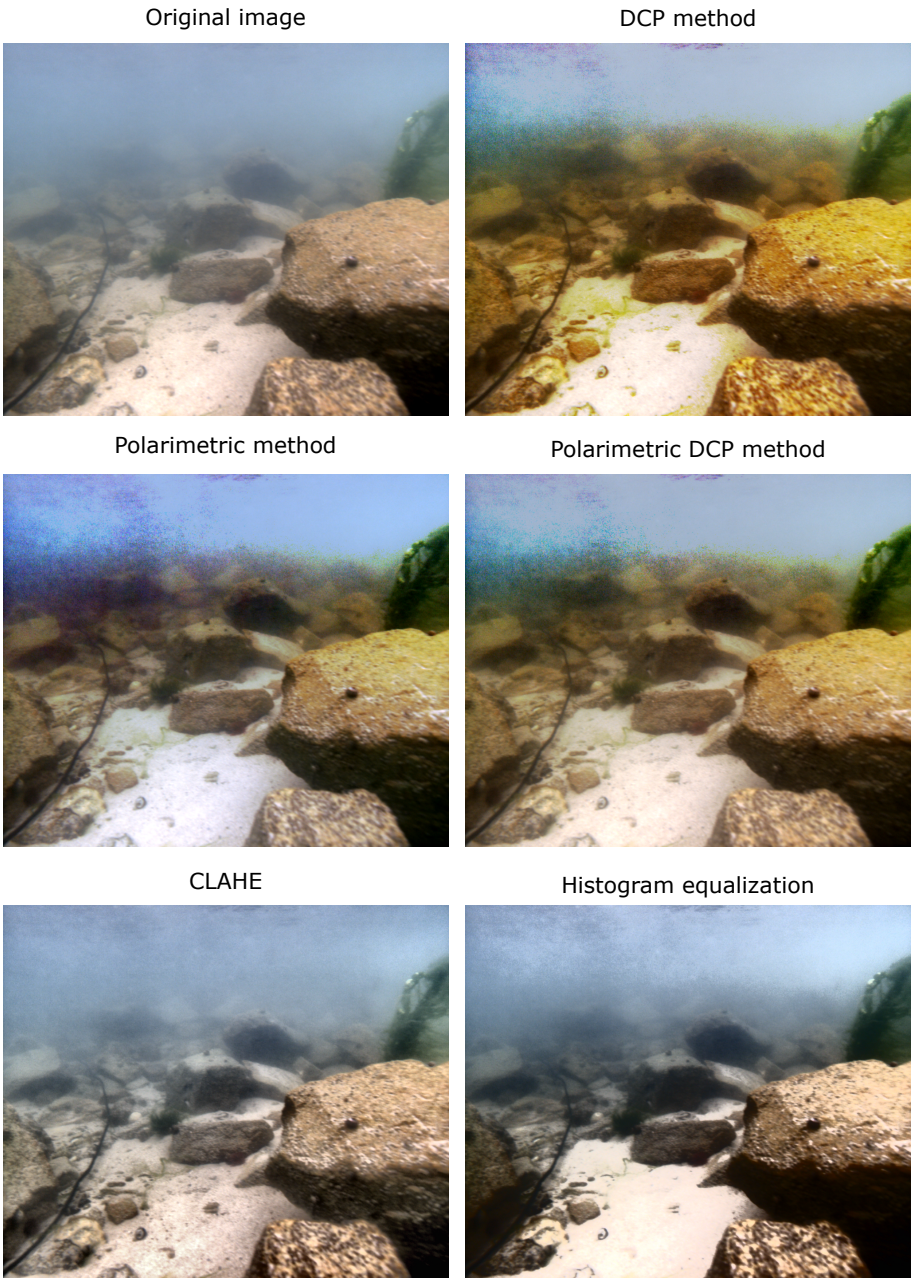


Fig. 4. Dehazing results on an image acquired using passive imaging. The original undehazed image is shown on the upper left corner. All the other images show the results of the corresponding method according to the protocol described in Section 6.2.

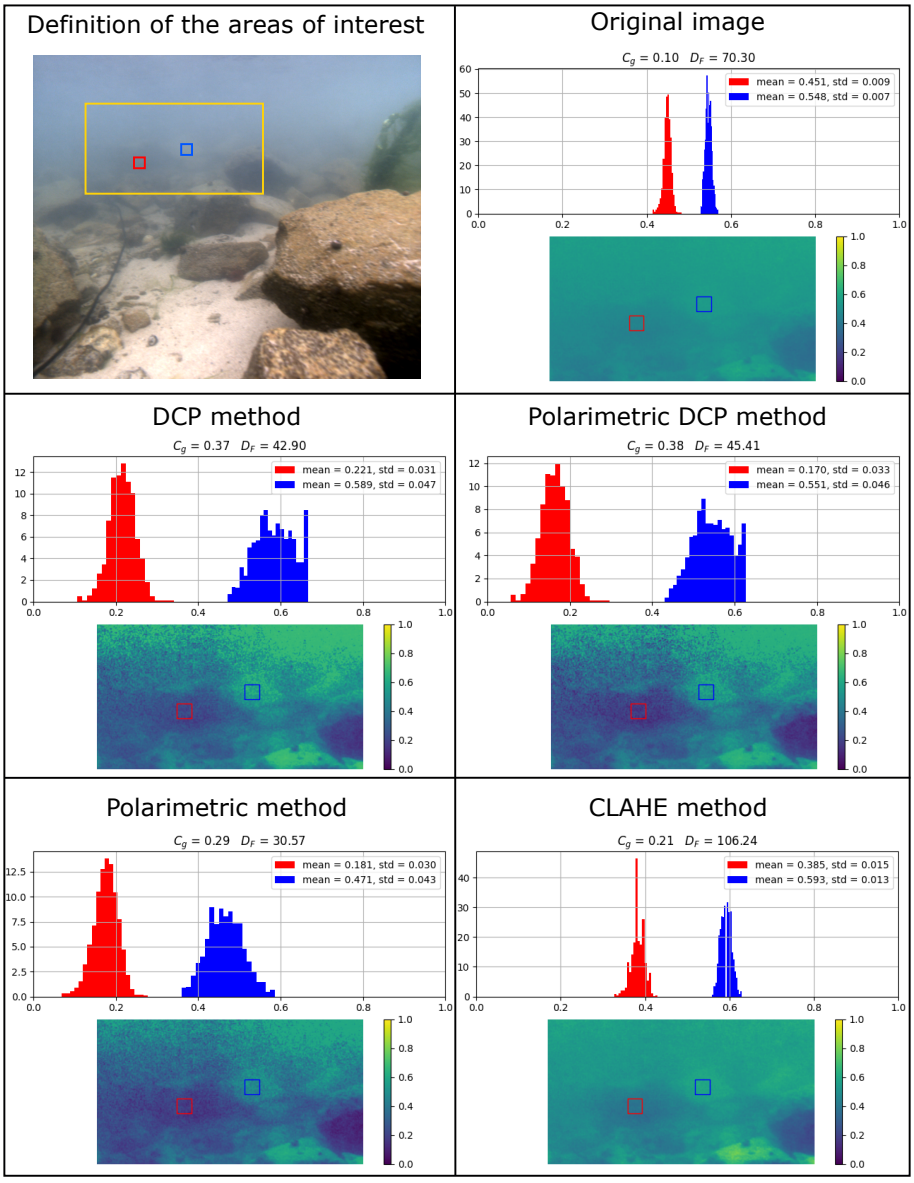


Fig. 5. Contrast between two zones on dehazed results of an image acquired with passive imaging. The image at the top left shows the full scene. The yellow rectangle indicates the zoomed-in region displayed in the other panels of the figure. The red and blue little squares mark the two regions used to compute the contrasts. The remaining panels in the figure present the results obtained with the different dehazing methods. The histograms corresponds to the pixel intensities within the red and blue regions. The mean values and standard deviations are reported in the legend. The subtitles indicate the values of the global contrast $C_g$ and the Fisher distance $D_F$. The zoomed-in region displayed in each panel and used for the metrics calculation shows the red channel of the corresponding dehazed image.

of concrete, while its upper part is made of a metallic tube topped with a white plastic cone. As one can see, the DCP, polarimetric and polarimetric DCP methods successfully remove a substantial portion of the scattering veil, except for a small region along the sides of the image. One can also notice that the polarimetric method attenuated the intensity from the metallic part of the mine, treating it as part of the veil. This effect arises because this metallic surface reflects polarized light similarly to the scattering veil. Therefore, the dehazing method attenuates the light reflected by this part of the mine as if it was due to scattering. This behavior is not observed with the DCP and polarimetric DCP methods. On the other hand, both CLAHE and histogram equalization enhance the contrast, but fail to suppress the veil, which remains prominent in the resulting images.

Figures 7 and 8 present the results of the calculation of the contrast metrics on the dehazed images displayed in Figure 6, using the same layout as in Figure 5. For both images, contrast values were computed between a specific part of the mine and the adjacent background. In Figure 7 the contrasts were computed for the metallic part of the mine whereas in Figure 8 the contrasts were computed for the white plastic cone at the top of the mine.

In Figure 7, the metal part of the mine is barely visible in the original image, resulting in a very low global contrast of 0.01 and a Fisher distance of 0.24. The DCP, polarimetric DCP and CLAHE methods enhance the global contrast to respectively 0.07, 0.08 and 0.07 and the Fisher distances to 8.25, 9.30 and 4.64. On the other hand, one can note that the polarimetric method does not improve contrast at all in this particular case. The global contrast remains as low as 0.01 and the Fisher distance decreases to 0.17. As previously discussed, the polarimetric method attenuates the light reflected by the metallic part in the same way it attenuates the veil. As a result, it fails to enhance the contrasts between the two regions. This example highlights the relevance of our polarimetric DCP method in addressing and mitigating such ambiguities.

In Figure 8, the white plastic cone remains distinguishable from the background despite the presence of the scattering veil in the original image. The global contrast is 0.09 and the Fisher distance reaches 61 in this case. The four dehazing methods significantly increase the global contrast to 0.18, 0.20, 0.24 and 0.23 respectively for the DCP, polarimetric DCP, polarimetric and CLAHE methods. While the first three slightly enhance the Fisher distance to respectively 74, 84 and 80, the CLAHE method increases it further to 132.

### *7.3. Discussion*

In this section, as well as in the other images we analyzed during our project, we observed that methods based on histogram equalization improve the global contrast of the images without effectively removing the scattering veil. In contrast, all dehazing methods based on physical priors—and for which the scene and the veil exhibit distinct properties—display similar behavior and effectively attenuate the veil. In particular, the combined use of the DCP method and polarimetric information through our polarimetric DCP approach has proven effective in resolving two key ambiguities: distinguishing the veil from a uniformly bright region, thereby allowing for an accurate selection of veil pixels to estimate its properties (cf. Figure 2); and differentiating a highly scattering region from the scattering veil (cf. Figure 8), while consistently ensuring strong dehazing performance across all studied cases.

As a result, the polarimetric DCP approach consistently produces results that are among the best across all tested methods. It therefore emerges as the most reliable and robust of the four approaches evaluated in this study.

### *7.4. Combination of DCP polarimetric and CLAHE*

Since the CLAHE method does not rely on any prior information about the scene nor the veil, it can be applied as a post-processing step following a dehazing method based on physical priors. We therefore propose its use after applying the polarimetric DCP method. The results obtained with

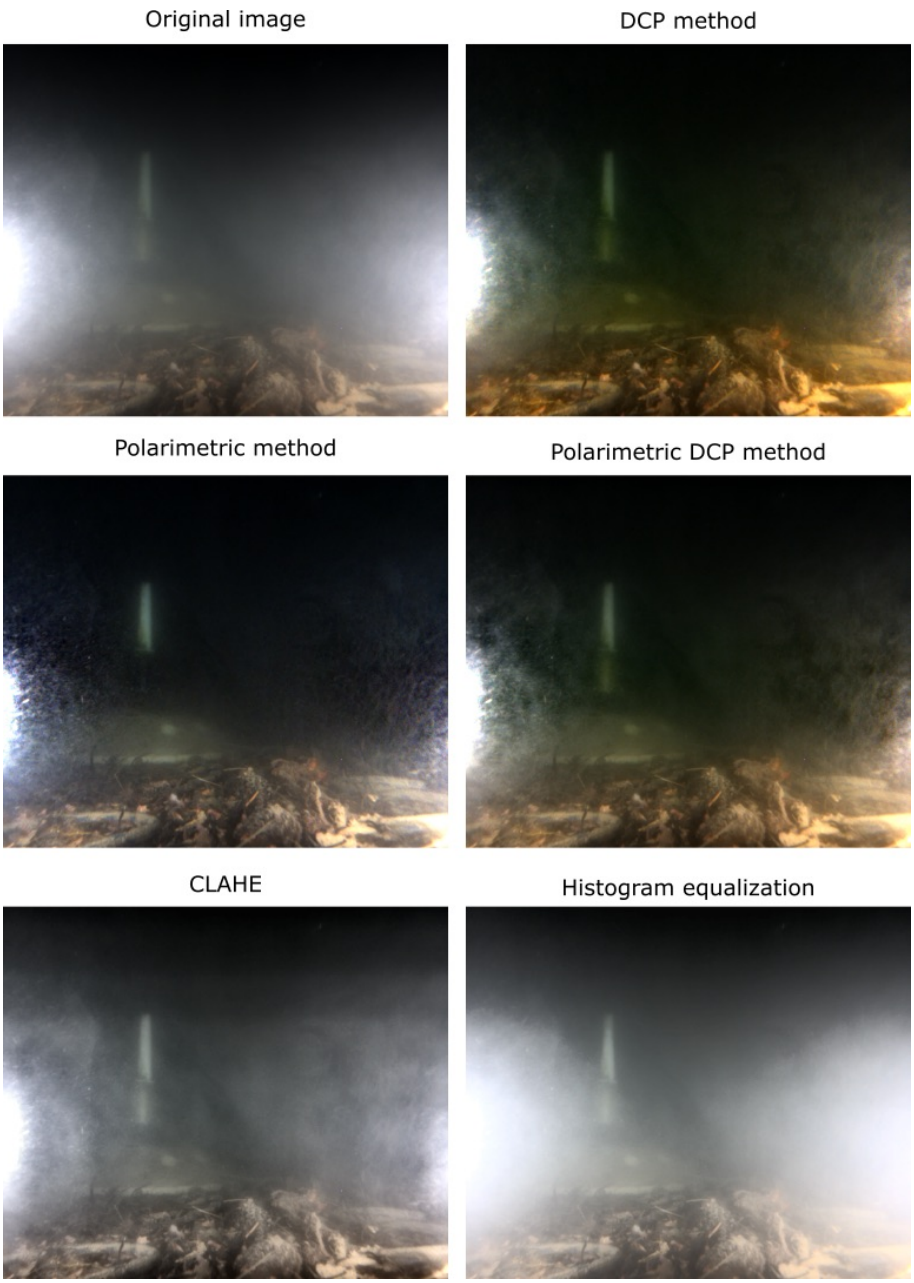


Fig. 6. Dehazing results of an image acquired using active imaging. The scene features a mine at approximately 1.5 m from the imaging system when the image was acquired. The original undehazed image is shown on the upper left. All the other images show the results of the corresponding method according to the protocol described in Section 6.2.

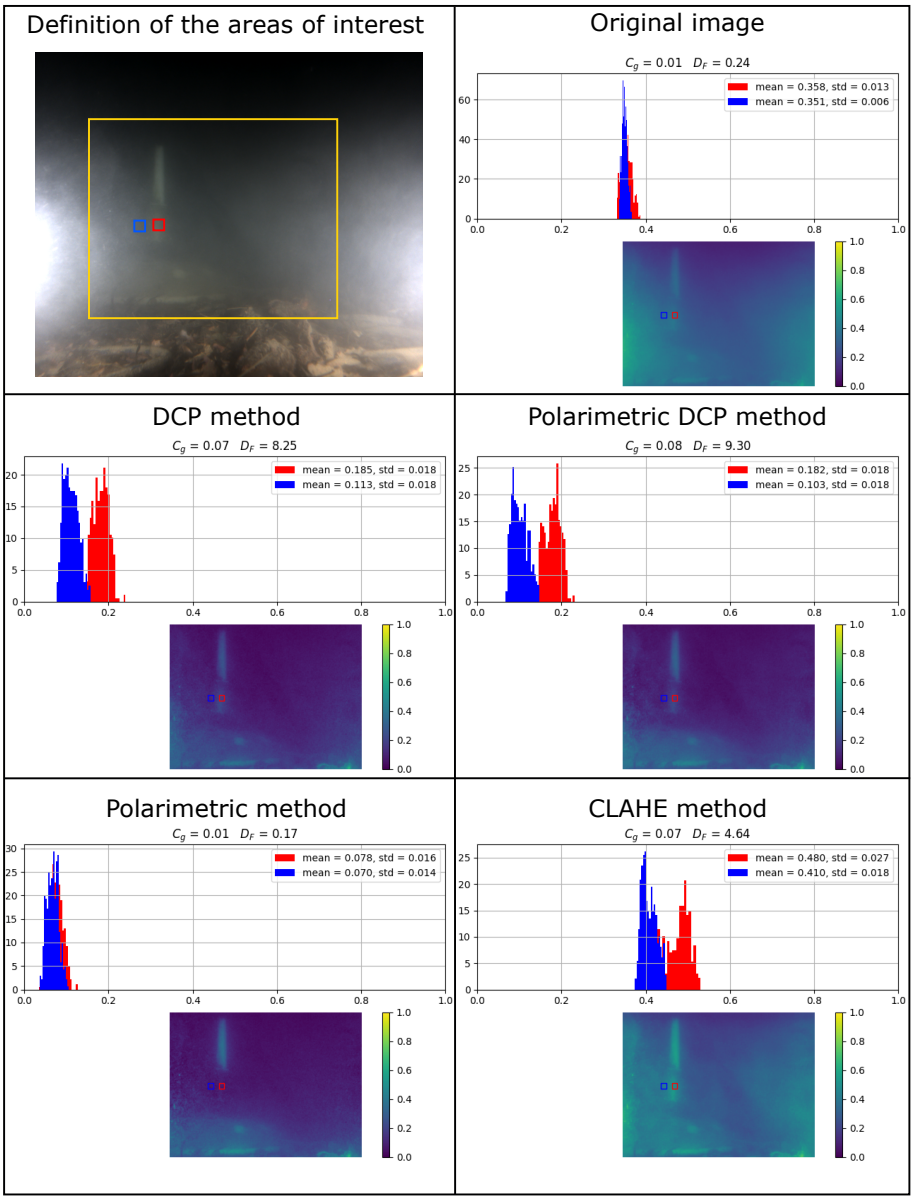


]

Fig. 7. Contrast between two zones on dehazed results of an image acquired with active imaging. The scene features a mine at approximately 1.5 m from the imaging system when the image was acquired. The contrasts are computed on the red channel and the layout follows the same pattern as in Figure 5.

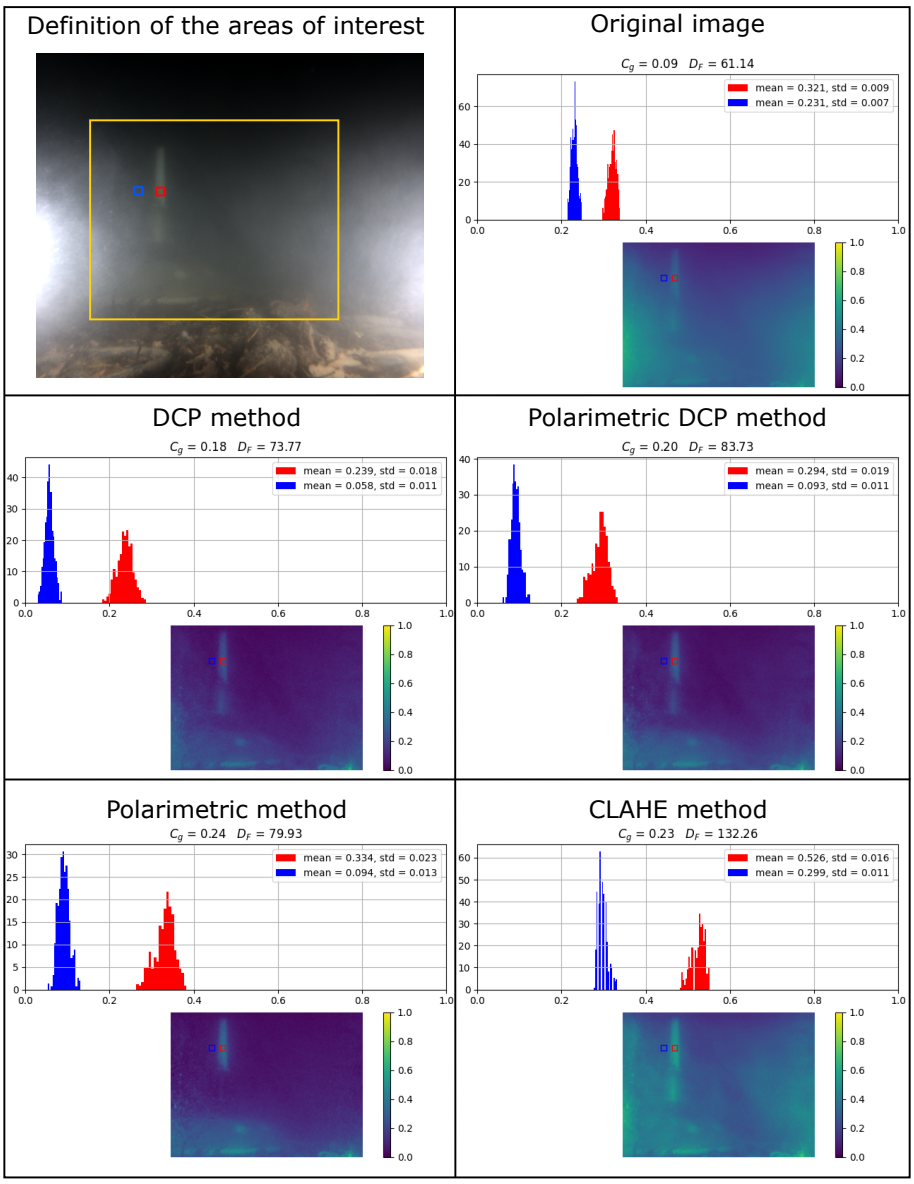


Fig. 8. Contrast between two zones on dehazed results of an image acquired with active imaging. The scene features a mine at approximately 1.5 m from the imaging system when the image was acquired. The contrasts are computed on the red channel and the layout follows the same pattern as in Figure 5.

this combined approach are presented in Figure 9. The left column shows the images produced by the polarimetric DCP method alone, while the right column displays the result of applying the CLAHE method to the output of the polarimetric DCP method. A significant improvement in visibility can be observed across all images, particularly in heavily hazed areas. As the CLAHE method does not remove the veil but substantially enhances contrast, its combination with the polarimetric DCP method—which effectively attenuates the scattering veil—yields dehazed images with markedly improved contrast.

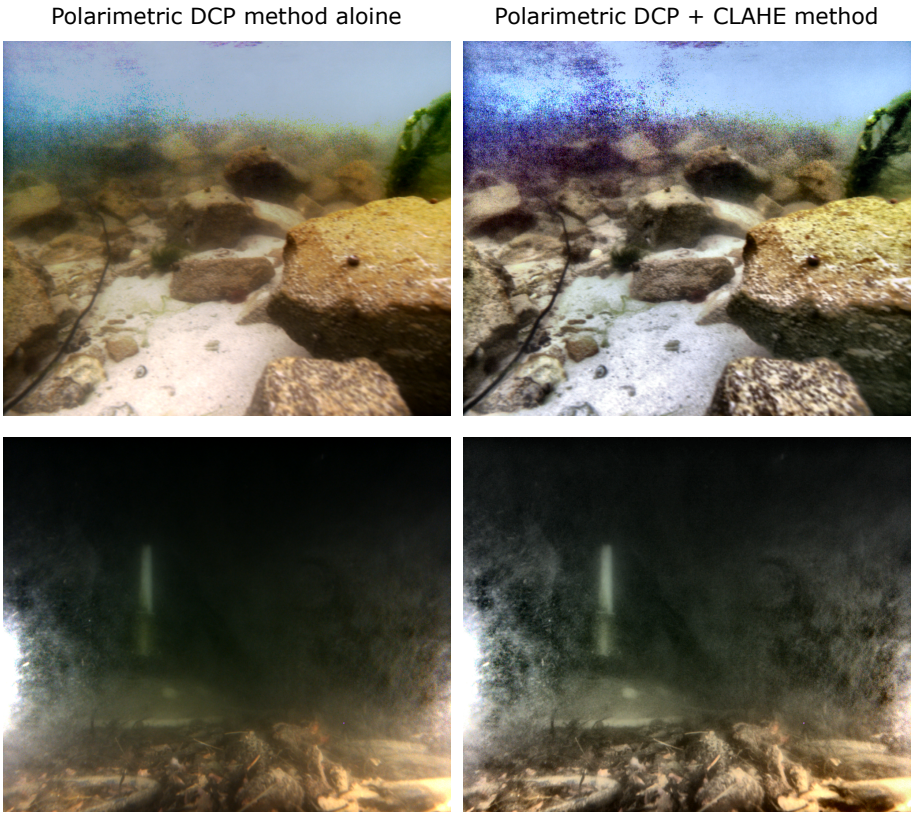


Fig. 9. Dehazing results with the polarimetric DCP method alone (left column) and with the the combination of the polarimetric DCP method followed by the CLAHE method (right column) for the two scenes presented in the previous subsections.

Figure 10 presents quantitative results of the CLAHE method, Polarimetric DCP method and their combination. Applying the two methods successively leads to a substantial improvement in both contrast metrics. The global contrast reaches a value of 0.21, which is two to three times higher than that obtained with either the CLAHE or the polarimetric DCP method alone. The Fisher distance is also noticeably increased in this example, further confirming the effectiveness of the combined approach.

## 8. Conclusion

We have developed a dehazing method which relies on and takes advantage of the dark channel prior of the DCP method and the polarimetric properties of the veil due to the scattering of light. This method allows to automatically and reliably selects the pixels in the image for which the scattering haze is the greatest and that can be used to estimate the parameters of the veil

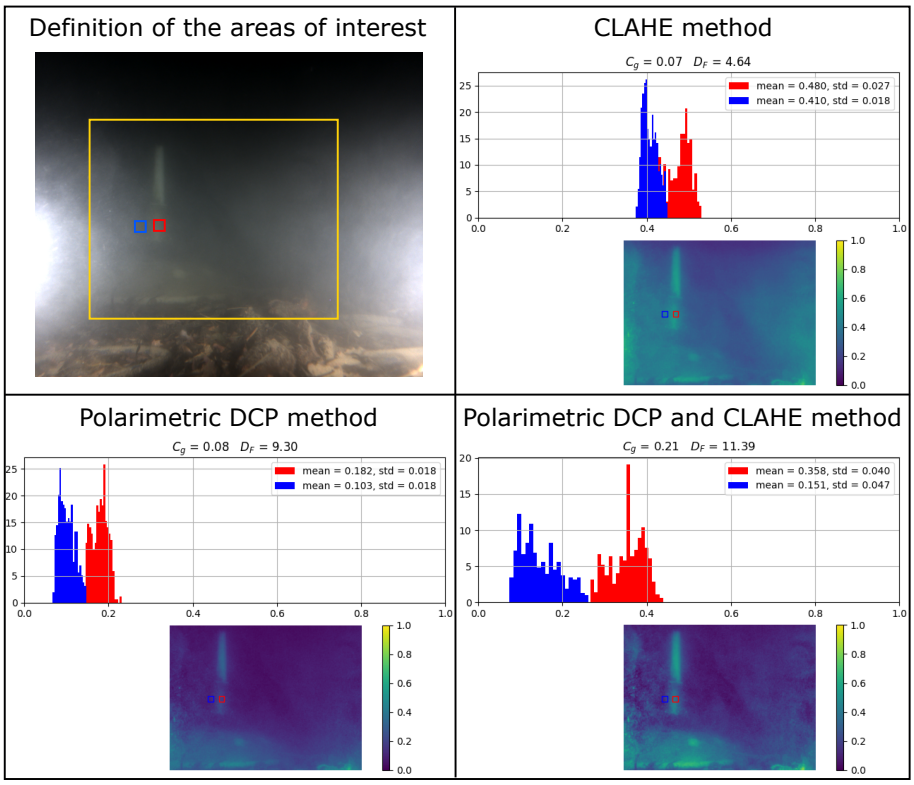


Fig. 10. Contrast between two zones on dehazed results of an image acquired with active imaging. The scene features a mine at approximately 1.5 m from the imaging system when the image was acquired. The contrasts are computed on the red channel and the layout follows the same pattern as in Figure 5.

necessary to perform the dehazing. It also allows to mitigate ambiguities between the veil and highly scattering part of the image, enabling image dehazing to be carried out reliably and with good performance across all the tests we performed. This method can be combined with the CLAHE method for even greater contrast enhancement. The performance of this method has been assessed on passive underwater images and on images acquired with an active underwater polarimetric imaging system embedded on a submarine drone. The images present different kind of scenes and we demonstrate that contrast enhancement can be achieved for all the situations explored in this study.

A natural perspective of this work would be to compare the performance of our algorithm to artificial intelligence dehazing methods and to tackle the issue of saturation artefacts that appears in the areas of the images where only the veil is present.

**Funding.** This work was supported by the French Ministry of Armed Forces – Agence de l'Innovation de Défense (AID) under the RAPID program, project POLSEA.

**Disclosures.** Arnaud Tullio: i2S (E). The imaging system used for this study was built by i2S according to the terms of the consortium agreement of the POLSEA research project. The authors declare no conflicts of interest.

**Data availability.** Data underlying the results presented in this paper are not publicly available at this time but may be obtained from the authors upon reasonable request.

## References


1. D. M. Kocak, F. R. Dalgleish, F. M. Caimi, and Y. Y. Schechner, "A focus on recent developments and trends in underwater imaging," Mar. Technol. Soc. J. **42**, 52–67 (2008).
2. S. M. Pizer, E. P. Amburn, J. D. Austin, *et al.*, "Adaptive histogram equalization and its variations," Comput. Vision, Graph. Image Process. **39**, 355–368 (1987).
3. B. Soni and P. Mathur, "An improved image dehazing technique using CLAHE and guided filter," 7th Int. Conf. on Signal Process. Integr. Networks (2020).
4. K. He, J. Sun, and X. Tang, "Single image haze removal using dark channel prior," IEEE Trans. on Pattern Anal. Mach. Intell. **33**, 2341–2353 (2011).
5. S. Li, F. Liu, and J. Wei, "Dehazing and deblurring of underwater images with heavy-tailed priors," Appl. Opt. **61**, 3855 (2022).
6. G. D. Gilbert and J. C. Pernicka, "Improvement of underwater visibility by reduction of backscatter with a circular polarization technique," Appl. Opt. **6**, 741 (1967).
7. Y. Y. Schechner, S. G. Narasimhan, and S. K. Nayar, "Polarization-based vision through haze," Appl. Opt. **42**, 511 (2003).
8. Y. Schechner and N. Karpel, "Clear underwater vision," IEEE Comput. Soc. Conf. on Comput. Vis. Pattern Recognit. (2004).
9. Y. Schechner and N. Karpel, "Recovering scenes by polarization analysis," Ocean. 04 MTS/IEEE Techno-Ocean 04 (2004).
10. Y. Schechner and N. Karpel, "Recovery of underwater visibility and structure by polarization analysis," IEEE J. Ocean. Eng. **30**, 570–587 (2005).
11. Y. Y. Schechner and Y. Averbuch, "Regularized image recovery in scattering media," IEEE Trans. on Pattern Anal. Mach. Intell. **29**, 1655–1660 (2007).
12. S. Shwartz, E. Namer, and Y. Schechner, "Blind haze separation," IEEE Comput. Soc. Conf. on Comput. Vis. Pattern Recognit. - Vol. 2 (2006).
13. X. Li, H. Hu, L. Zhao, *et al.*, "Pseudo-polarimetric method for dense haze removal," IEEE Photonics J. **11**, 1–11 (2019).
14. T. Treibitz and Y. Schechner, "Instant 3descatter," IEEE Comput. Soc. Conf. on Comput. Vis. Pattern Recognit. - Vol. 2 (2006).
15. T. Treibitz and Y. Schechner, "Active polarization descattering," IEEE Trans. on Pattern Anal. Mach. Intell. **31**, 385–399 (2009).
16. B. Huang, T. Liu, H. Hu, *et al.*, "Underwater image recovery considering polarization effects of objects," Opt. Express **24**, 9826 (2016).
17. H. Li, J. Zhu, J. Deng, *et al.*, "Visibility enhancement of underwater images based on polarization common-mode rejection of a highly polarized target signal," Opt. Express **30**, 43973 (2022).
18. H. Zhang, M. Ren, H. Wang, *et al.*, "Fast processing of underwater polarization imaging based on optical correlation," Appl. Opt. **60**, 4462 (2021).
19. Y. Wei, P. Han, F. Liu, and X. Shao, "Enhancement of underwater vision by fully exploiting the polarization information from the stokes vector," Opt. Express **29**, 22275 (2021).
20. F. Huang, C. Ke, X. Wu, *et al.*, "Polarization dehazing method based on spatial frequency division and fusion for a far-field and dense hazy image," Appl. Opt. **60**, 9319 (2021).
21. R. Sun, T. Liao, Z. Fan, *et al.*, "Polarization dehazing method based on separating and iterative optimizing airlight from the frequency domain for different concentrations of haze," Appl. Opt. **61**, 10362 (2022).
22. T. Yamazaki, Y. Maruyama, Y. Uesaka, *et al.*, "Four-directional pixel-wise polarization CMOS image sensor using air-gap wire grid on 2.5-$\mu$m back-illuminated pixels," IEEE Int. Electron Devices Meet. (2016).
23. T. Li, J. Wang, and K. Yao, "Visibility enhancement of underwater images based on active polarized illumination and average filtering technology," Alex. Eng. J. **61**, 701–708 (2022).
24. H. Suo, J. Guan, M. Ma, *et al.*, "Dynamic dark channel prior dehazing with polarization," Appl. Sci. **13**, 10475 (2023).
25. H. Zhang, "single image dehaze," https://github.com/He-Zhang/image_dehaze.
26. K. He, J. Sun, and X. Tang, "Guided image filtering," IEEE Trans. on Pattern Anal. Mach. Intell. **35**, 1397–1409 (2012).
27. B. Le Teurnier, N. Li, M. Boffety, and F. Goudail, "Definition of an error map for DOFP polarimetric images and its application to retardance calibration," Opt. Express (2022).
28. B. Le Teurnier, M. Boffety, and F. Goudail, "Error model for linear DoFP imaging systems perturbed by spatially varying polarization states," Appl. Opt. (2022).
29. i2S, Orphiecam 300, https://i2s-orphie.com/produits-orphiecam300/.
30. K. J. Voss and E. S. Fry, "Measurement of the mueller matrix for ocean water," Appl. Opt. **23**, 4427–4439 (1984).
31. F. Goudail, P. Réfrégier, and G. Delyon, "Bhattacharyya distance as a contrast parameter for statistical processing of noisy optical images," J. Opt. Soc. Am. A **21**, 1231 (2004).
32. N. Vannier, F. Goudail, C. Plassart, *et al.*, "Comparison of different active polarimetric imaging modes for target detection in outdoor environment," Appl. Opt. **55**, 2881 (2016).